Ionic-passivated FeS_2 photocapicitors for energy conversion and storage

by Maogang Gong et al.

2013

ChemComm

RSC Publishing

COMMUNICATION

View Article Online
View Journal | View Issue

Ionic-passivated FeS_2 photocapacitors for energy conversion and storage†

Cite this: *Chem. Commun.*, 2013, **49**, 9260

Received 6th July 2013,
Accepted 8th August 2013

DOI: 10.1039/c3cc45088k

www.rsc.org/chemcomm

Maogang Gong,[a] Alec Kirkeminde,[a] Nardeep Kumar,[b] Hui Zhao[b] and Shenqiang Ren*[a]

A solid-state photocapacitor is prepared, utilizing iron pyrite (FeS_2) as both the photoactive material and blocking electrode, which exhibits a high performance near-infrared (NIR) photodetectivity of 1.6×10^{11} Jones, an energy density of 1.13×10^4 J g^{-1} and a specific capacitance of 37.5 mA h g^{-1} directly charged by sunlight.

With the emergence of and rapid demand for solar energy utilization, it has become necessary to develop a more suitable method for simultaneous sunlight conversion and storage. Both photovoltaics (PVs) and batteries/supercapacitors, developed as independent technologies, have been separately proposed to help meet this demand. However, integrating energy conversion and storage is a challenging task. Recently, a type of capacitor that can be charged by solar radiation has been shown, which was deemed a "photocapacitor".[1] Photocapacitors (PCs), as the name suggests, are capacitors that are charged utilizing solar light, which allows for direct storage of solar energy. Most photocapacitors utilize a hybrid setup which consists of a dye-sensitized cell using standard TiO_2 decorated with a dye and an electrolyte, providing electrons to charge a separate carbon electrode–electrolyte capacitor system.[2] Therefore, it would be advantageous to simplify this setup, by having one material–electrolyte system that simultaneously acts as the active material and blocking electrode. In this study, we present a solution processed photocapacitor that makes use of earth abundant iron pyrite (FeS_2) nanocrystals to achieve this goal.

Earth abundant FeS_2 nanomaterials have been widely proposed in renewable energy applications, such as PVs,[3,4] energy storage batteries[5] and photocatalysts.[6] More recently, FeS_2 has been integrated into photodetectors that can function in the near-infrared (NIR) range.[7] Interest has been peaked due to pyrite's strong absorption ($\alpha > 10^5$ cm^{-1} in visible), reasonable band gap ($E_g \sim 0.95$ eV), low toxicity and being outstandingly earth abundant.[3,8] However, despite all of these exceptional qualities, the development of pyrite-based energy applications has been limited, such as PV devices. The champion pyrite PV cell is a photoelectrochemical device reported in 1991 and no further improvements have been made since.[9] It is believed that pyrite is being suppressed by defect states (sulfur vacancies) and metallic and semi-metallic polymorphs of other iron sulfides existing in the material where phase purity is needed.[10,11] Many studies have been suggested as a means to deal with defect states, such as colloidal growth to keep crystallinity high or highly controlled chemical vapor deposition thin film growth.[6,12] Passivation of surface defects could help with the proposed pinning of the Fermi level,[11,13] but it needs to be done in a way that doesn't inhibit charge transport. Tributsch *et al.* showed the optimized performance of photoelectrochemical cells utilizing an I^-/I_3 electrolyte, which was attributed to the adsorption of ions onto the active material surface.[3] Halide ions have strong affinity for the Fe-terminated cations of FeS_2 (100) surfaces and act as ligands offering a direct approach to highly effective passivation.[14] While this was beneficial, having an aqueous electrolyte solution is detrimental to pyrite due to its known photo-degradation in water.[15] Therefore, utilizing an anhydrous source of I^-, from ionic liquids (IL) in this study, could provide the pyrite passivation and still allow charge transfer with minimal degradation. The physical and chemical properties of ILs could also be readily tuned *via* varying the nature of cations/anions, which have found applications in dye-sensitized solar cells,[16] LIBs[17] and green solvents.[18]

In this report, we demonstrate a pyrite photocapacitor that is capable of cyclic charge–discharge with an energy density of 1.13×10^4 J g^{-1}. The device utilizes ionic liquids to passivate surface states on the pyrite nanocrystals to enhance carrier lifetime, which is characterized using ultrafast pump–probe measurements. This observation takes a step forward in helping to solve the pyrite's surface defect problem. The ionic liquid also plays the role of the electrolyte in this electric double layer capacitor. Charging of the FeS_2 photocapacitor is seen to occur due to the photocurrent generation of the active pyrite material under broad spectral sunlight absorption. This is the first report of a truly hybridized photocapacitor, where the active material of pyrite works as both the photocharging material and the blocking electrode.

[a] *Department of Chemistry, University of Kansas, Lawrence, KS 66045, USA. E-mail: shenqiang@ku.edu; Tel: +1-785-864-2315*

[b] *Department of Physics, University of Kansas, Lawrence, KS 66045, USA*

† Electronic supplementary information (ESI) available: XRD characterization, additional TEM images, schematic of detector instrumentation, FTIR spectrum, photocurrent comparison, cyclic voltammograms, charge–discharge *V–t* characteristics. See DOI: 10.1039/c3cc45088k

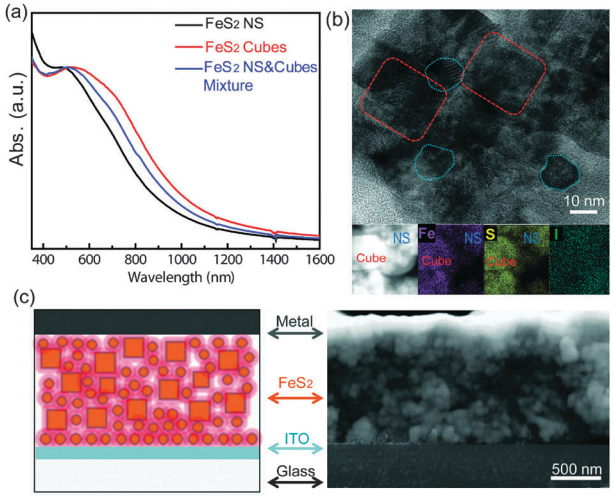

Fig. 1 (a) UV-Vis-NIR absorbance of FeS_2 NS, cubes and mixed. (b) TEM and EDS mapping images of FeS_2 NS–cube mixture capped by BMII. (c) Schematic device structure and cross-sectional SEM image of the FeS_2 NS–cube devices.

The mineral iron pyrite is an iron disulfide with the formula FeS_2 (Fig. S1, ESI†). We have shown that the Fe-terminated [100] surface facet dominant colloidal growth results in cubic structures.[6] The X-ray diffraction (XRD, Fig. S2, ESI†) pattern of the FeS_2 nanocrystals is consistent with the pyrite structure (JCPDS Card No 1-079-0617), without detectable marcasite, greigite, pyrrhotite, or other impurities. Fig. 1a shows the absorption spectra of FeS_2 nanocrystals (nanospheres: NS, nanocubes: cube, and their mixture), which demonstrate promising light harvesting capabilities across the visible to NIR spectrum.

Much attention has been devoted to the development of new ligand strategies that minimize the interparticle spacing and enhance electronic coupling to promote carrier transport. These new strategies could also help avoid surface defect recombination loss. The quantum dot PVs have been realized using a variety of short mono- and bidentate organic ligands. Ethanedithiol (EDT), aromatic thiols,[19] alkylamines,[20] mercaptocarboxylic acids (MPA)[21] and inorganic ligands[14] have all shown promise in achieving effective passivation while reducing interparticle spacing. We have utilized three different ligands to examine their passivation effects on the performance of FeS_2 photocapacitors. The EDT ligand is examined as a reference to compare with the halide based IL passivation effects. The other two halide based ILs include 1-hexyl-3-methylimidazolium bromide ([Hmim][Br]) and 1-butyl-3-methylimidazolium iodide (BMII). After the halide atomic ligand exchange, transmission electron microscopy (TEM) is used to investigate the stability of FeS_2 nanocrystals without noticeable shape change. The BMII-treated FeS_2 NS and cube mixture is shown in Fig. 1b. The FeS_2 NS and cubes exhibit on average 13.4 nm diameter and 47.5 nm side length, respectively. A high resolution TEM (HRTEM) image shows the lattice fringe of FeS_2 nanocrystals with the lattice spacing of 0.27 nm, matching the (200) plane of pyrite (see Fig. S3, ESI†). The scanning TEM-energy dispersive X-ray spectrometry (STEM-EDS) images show the elemental mapping of the iodide passivated FeS_2 nanocrystals. Fig. 1c shows a schematic of ionic liquid treated FeS_2 hybrid photocapacitor devices produced in this study, along with the cross-sectional SEM image of the device for comparison. It can be seen that the FeS_2 NS form a matrix around the FeS_2 cubes, which produce a close-packed structure and the resulting nano-porosity is further backfilled by the spun-cast halide based IL to allow for efficient charge transfer and transport. The atomic force microscope (AFM) cross-sectional image of the FeS_2 photocapactior device further confirms the well-distributed FeS_2 nanocrystals stacked between two electrodes to form the active layer (Fig. S1b, ESI†).

It is known that FeS_2 materials have relatively scattered electrical properties due to the formation of surface defects related to sulfur vacancies[10] and oxygen absorbance.[22] These problems could be exacerbated in the nanocrystal devices due to the high concentration of interfaces. The performance improvement shown here with the addition of the halide for atomic ligand passivation motivated us to investigate and understand charge carrier dynamics, lifetime and related carrier density by the surface passivation effect. An optical ultrafast pump–probe technique is used to measure the carrier lifetime (the schematic ultrafast laser set-up is shown in Fig. S4, ESI†). Fig. 2a and b show the measured reflection signal as a function of the probe delay (the arriving time of the probe pulse at the sample with respect to the pump pulse), corresponding to FeS_2 NS–cube mixture PC devices treated with the BMII, [Hmim][Br], respectively. The Fourier transform infrared spectroscopy (FTIR) confirms that the halide atomic ligand treatment of FeS_2 nanocrystals enables the removal of surface insulating organic ligands (Fig. S5, ESI†). The measured decay time can be attributed to the carrier lifetime of FeS_2 nanocrystals.[23] The signal decays exponentially, so by fitting the curve, the carrier lifetime of the passivated FeS_2 nanocrystals can be obtained. The EDT (inset of Fig. 2c), [Hmim][Br] and [BMII] treated PC devices show the carrier lifetime of 8 ps, 126 ps and 189 ps, respectively. Fig. 2c summarizes the carrier lifetime of FeS_2 nanocrystals in relation to different passivation schemes. The ultrashort lifetime of the EDT-treated device is consistent with the low photocurrent measured (Fig. S6, ESI†). The halide ligand-passivated devices, with longer carrier lifetimes and higher photocurrent, can be attributed to the passivation of FeS_2 surface defect states and fast carrier transport. A similar halide compound passivation effect has also been reported by Sargent *et al.*,[14] where the Br-capped PbS devices showed one order of magnitude faster mobility than that of MPA- and EDT-treated films.

We expect that the ionic passivation of FeS_2 nanocrystals could facilitate their photoresponse behavior, under the 1100 nm NIR illumination shown in Fig. S7a (ESI†). It should be noted that the NIR light source used here can be used to photoexcite FeS_2 only.

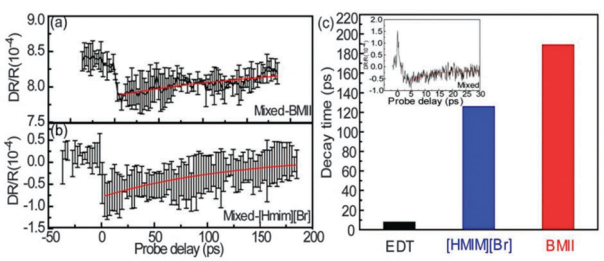

Fig. 2 Differential reflection measured from FeS_2 NS–cube films passivated by (a) BMII: 189 ps lifetime, (b) [Hmim][Br]: 126 ps lifetime, and (c) the decay time related with different passivation schemes (the inset is the differential reflection exhibiting the EDT passivated control sample: 9 ps lifetime).

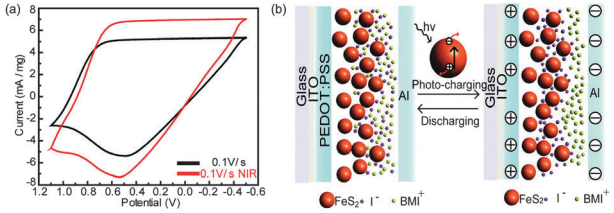

Fig. 3 (a) The cyclic voltammetry curves of FeS_2 photocapacitors at scan rates of 0.1 V s^{-1}, under room ambient light (as ''dark'') and 1100 nm NIR illumination (as ''light''). (b) The schematic image of the operating principle of FeS_2 photocapacitors.

The high performance BMII-passivated FeS_2 photocapacitors show a photoresponse of 37.6 A W^{-1} and photodetectivity of 1.6×10^{11} under 1100 nm illumination. The responsivity is one order of magnitude lower compared to bulk-nanojunction FeS_2/CdS photodetectors (174.9 A W^{-1})[7] and one order of magnitude higher than that of the organic–inorganic blend of PbS/PCBM photodetectors (1.6 A W^{-1}).[24] With the aim of testing FeS_2 photocharging ability, we evaluate the electrochemical capacitance measurements of FeS_2 photocapacitors under 1100 nm NIR light, and the cyclic voltammogram of FeS_2 photocapacitors is shown in Fig. 3a. The specific capacities (C_s) of 37.5 mA h g^{-1} under room ambient light (as "dark") and 46.0 mA h g^{-1} under the 1100 nm NIR illumination (as "light") are shown in Fig. 3a. The specific capacity increases by 23% under the NIR light illumination, which confirms the photocharging from NIR photoresponsive FeS_2 nanocrystals. The FeS_2 photocapacitors are also tested at different scan rates (Fig. S7b, ESI†).

We interpret the operating principle of FeS_2 photocapacitors as following (Fig. 3b). Under the room ambient light conditions (as "dark"), the ionic liquid does not experience much charge separation, limited mostly to I^- being adsorbed onto the Fe^{2+}-rich defect sites of the FeS_2 nanocrystals. Under light illumination, the p-type FeS_2 nanocrystals are photo-excited, leading to the hole generation and transport resulting in partial positive charge on the FeS_2 nanocrystals. More I^- ions are then attracted to the FeS_2 surface by the columbic force, leaving behind the cation thus creating the separation of charge. This photocharging is exclusively due to the photoexcitation of FeS_2 nanocrystals. When the light is then switched off, the double layer dissipates and is discharged under the bias voltage. To understand the size effect of different ions on the transport properties of FeS_2 photocapacitors, we select an ionic liquid with a bigger anion ($[Tf_2N]^-$). The current-time and the voltage-time characteristics of the FeS_2 photocapacitor modified with [BMII] and [Hmim][Tf_2N] are shown in Fig. S8 (ESI†), respectively. The rate of discharge is seen to change between the two electrolytes, where I^- charges faster than the bigger [Tf_2N] due to the proportionality of the mobility to the radius of ions ($v \approx 1/r^2$). When the small sized I^- is used, it can passivate FeS_2 nanocrystals more effectively and move faster, which allows it to exhibit higher capacity and a fast discharging rate. The photon-induced energy stored in the capacitor can be calculated by integrating I–t curves (current intensity reaches saturation under AM-1.5 light illumination). According to $W_{stored} = QU = U\int\int didt$, where W_{stored}, Q, U, i and t are the storage energy, electrical quantity, applied voltage, current and time, the photocharged energy density was calculated as 1.13×10^4 J g^{-1} for the BMII-based photocapacitor and 0.3×10^4 J g^{-1} for the [Hmim][Tf_2N]-based photocapacitor. The former is nearly 4 times that of the latter case, which further confirms the ionic size effect on the transport and capacitance of photocapacitors. This can be partially attributed to the steric effect of the larger size of the [Tf_2N] ions, reducing the energy density from the electric double layer capacitors.

In summary, we have demonstrated the photocapacitors that utilize the FeS_2 nanocrystals as both the photocharging source and the blocking electrode. It is also shown that ionic liquids can serve well in photocapacitors for the formation of the electric double layer, and more importantly, can be used to passivate the surface states of FeS_2 nanomaterials to enhance charge transport, which can allow for better devices to be made from the promising earth abundant material. We also find that the size of ions plays an integral role in the energy density of the photocapacitor devices. The FeS_2 photocapacitor devices exhibit an energy density and a specific capacity of 1.13×10^4 J g^{-1} and 37.5 mA h g^{-1} respectively, which show promise for construction of direct solar energy storage devices.

S.R. thanks the financial support from the National Science Foundation under Award No. NSF-CMMI-1332658 for material synthesis and assembly, Department of Energy award (DE-FG02-13ER46937) for the physical property characterization, and the University of Kansas New Faculty General Research Fund.

Notes and references

1 T. Miyasaka and T. N. Murakami, *Appl. Phys. Lett.*, 2004, **85**, 3932.
2 Z. Yang, L. Li, Y. Luo, R. He, L. Qiu, H. Lin and H. Peng, *J. Mater. Chem. A*, 2013, **1**, 954.
3 A. Ennaoui, S. Fiechter, C. Pettenkofer, N. Alonsovante, K. Buker, M. Bronold, C. Hopfner and H. Tributsch, *Sol. Energy Mater. Sol. Cells*, 1993, **29**, 289.
4 A. Kirkeminde, R. Scott and S. Ren, *Nanoscale*, 2012, **4**, 7649.
5 J.-W. Choi, G. Cheruvally, H.-J. Ahn, K.-W. Kim and J.-H. Ahn, *J. Power Sources*, 2006, **163**, 158.
6 A. Kirkeminde and S. Ren, *J. Mater. Chem. A*, 2013, **1**, 49.
7 M. G. Gong, A. Kirkeminde, Y. Xie, R. Lu, J. Liu, J. Z. Wu and S. Ren, *Adv. Opt. Mater.*, 2013, **1**, 78.
8 P. P. Altermatt, T. Kiesewetter, K. Ellmer and H. Tributsch, *Sol. Energy Mater. Sol. Cells*, 2002, **71**, 181.
9 V. Antonucci, A. S. Arico, N. Giordano, P. L. Antonucci, U. Russo, D. L. Cocke and F. Crea, *Sol. Cells*, 1991, **31**, 119.
10 C. Steinhagen, T. B. Harvey, C. J. Stolle, J. Harris and B. A. Korgel, *J. Phys. Chem. Lett.*, 2012, **3**, 2352.
11 M. Birkholz, S. Fiechter, A. Hartmann and H. Tributsch, *Phys. Rev. B*, 1991, **43**, 11926.
12 J. Puthussery, S. Seefeld, N. Berry, M. Gibbs and M. Law, *J. Am. Chem. Soc.*, 2010, **133**, 716.
13 B. Thomas, K. Ellmer, M. Muller, C. Hopfner, S. Fiechter and H. Tributsch, *J. Cryst. Growth*, 1997, **170**, 808.
14 J. Tang, K. Kemp, S. Hoogland, K. Jeong, H. Liu, L. Levina, M. Furukawa, X. Wang, R. Debnath, D. Cha, K. Chou, A. Fischer, A. Amassian, J. Asbury and E. Sargent, *Nat. Mater.*, 2011, **10**, 765.
15 P. J. Sullivan, J. L. Yelton and K. J. Reddy, *Environ. Geol. Water Sci.*, 1988, **11**, 289.
16 S. Ito, S. M. Zakeeruddin, P. Comte, P. Liska, D. Kuang and M. Gratzel, *Nat. Photonics*, 2008, **2**, 693.
17 A. Lewandowski and A. Świderska-Mocek, *J. Power Sources*, 2009, **194**, 601.
18 L. A. Blanchard, D. Hancu, E. J. Beckman and J. F. Brennecke, *Nature*, 1999, **399**, 28.
19 G. I. Koleilat, L. Levina, H. Shukla, S. Myrskog, S. Hinds, A. G. Pattantyus-Abraham and E. Sargent, *ACS Nano*, 2008, **2**, 833.
20 D. V. Talapin and C. B. Murray, *Science*, 2005, **310**, 86.
21 A. Pattantyus-Abraham, I. Kramer, A. Barkhouse, X. Wang, G. Konstantatos, R. Debnath, L. Levina, I. Raabe, M. Nazeeruddin, M. Grätzel and E. Sargent, *ACS Nano*, 2010, **4**, 3374.
22 R. Sun, M. K. Y. Chan, S. Kang and G. Ceder, *Phys. Rev. B*, 2011, **84**, 035212.
23 A. Kirkeminde, B. Ruzicka, R. Wang, S. Puna, H. Zhao and S. Q. Ren, *ACS Appl. Mater. Interfaces*, 2012, **4**, 1174.
24 K. Szendrei, F. Cordella and M. A. Loi, *Adv. Mater.*, 2009, **21**, 683.

